

Journal of Marine Research
A Contribution to Honor Nick Fofonoff
2/1/2005

Deep Ocean Experiments with Fossil Fuel Carbon Dioxide: Creation and
Sensing of a Controlled Plume at 4 km Depth.

By

Peter G. Brewer¹, Edward T. Peltzer¹, Peter Walz¹, Izuo Aya², Kenji Yamane², Ryuji Kojima², Yasuharu Nakajima³, Noriko Nakayama⁴, Peter Haugan⁵, and Truls Johannessen⁵.

1. Monterey Bay Aquarium Research Institute, Moss Landing, CA 95039 USA.
2. Osaka Branch, National Maritime Research Institute, 3-5-10 Amanogahara, Katano, Osaka 576-0034, Japan.
3. Main Branch, National Maritime Research Inst. (NMRI), 6-38-1 Sinkawa, Mitaka, Tokyo 181-0004, Japan.
4. Ocean Research Institute, University of Tokyo, 1-15-1 Minamidai, Nakano-ku, Tokyo 168-8639, Japan.
5. University of Bergen, Allegaten 70, N-5007 Bergen, Norway.

Abstract

The rapidly rising levels of atmospheric and oceanic CO₂ from the burning of fossil fuels has lead to well-established international concerns over dangerous anthropogenic interference with climate. Disposal of captured fossil fuel CO₂ either underground, or in the deep ocean, has been suggested as one means of ameliorating this problem. While the basic thermodynamic properties of both CO₂ and seawater are well known, the problem of interaction of the two fluids in motion to create a plume of high CO₂/low pH sea water has been modeled, but not tested. We describe here a novel experiment designed to initiate study of this problem. We constructed a small flume, which was deployed on the sea floor at 4 km depth by a remotely operated vehicle, and filled with liquid CO₂. Sea water flow was forced across the surface by means of a controllable thruster. Obtaining quantitative data on the plume created proved to be challenging. We observed and sensed the interface and boundary layers, the formation of a solid hydrate, and the low pH/high CO₂ plume created, with both pH and conductivity sensors placed downstream. Local disequilibrium in the CO₂ system components was observed due to the finite hydration reaction rate, so that the pH sensors closest to the source only detected a fraction of the CO₂ emitted. The free CO₂ molecules were detected through the decrease in conductivity observed, and the disequilibrium was confirmed through trapping a sample in a flow cell and observing an unusually rapid drop in pH to an equilibrium value.

1. Introduction

Background

The extraordinary rise in fossil fuel CO₂ concentrations in both the atmosphere (IPCC, 1990, 1996) and the oceans (Brewer, 1978; Sabine et al., 2002) and the associated problem of climate change, has led to debate over possible solutions. Some 30% of the CO₂ disposed of in the atmosphere is rapidly transferred to the ocean through gas exchange, and in the very long term the ocean will take up some 85% of all fossil fuel emissions. It was this that led Marchetti (1977) to suggest direct deep ocean injection of CO₂ as a possible solution to the climate problem. This theme has been revisited many times, notably by the U.S. President's Council of Advisors on Science and Technology (PCAST, 1997) who issued a report recommending storage of CO₂ as a hydrate on the ocean floor. The PCAST report indicated a belief that, since the temperature and pressure conditions in the deep ocean favor formation of a solid CO₂ hydrate (CO₂·6H₂O), the solid once formed would be thermodynamically stable.

There have now been many analyses of the behavior of CO₂ within the oceanic hydrate-forming regime, and the complexity this introduces (Haugan and Drange, 1992; Cole et al., 1993; Stegen et al., 1993; Morishita et al., 1993; Shindo et al., 1993; Handa and Ohsumi, 1995). Small-scale laboratory experiments have been carried out in Japan (Aya et al., 1992; Kimuro et al., 1993; Ohgaki et al., 1993; Ozaki et al., 1993; Saito et al., 1995; Kobayashi et al., 1995), and in the US (Masutani et al., 1993) to investigate this problem. Nakashiki et al. (1991) conducted the first field experiment using solid CO₂ (dry ice) and measured its descending velocity. Aya et al. (1993) made laboratory measurements of the dissolution rate of a static hydrate-coated CO₂ droplet. Brewer et al. (2002) made field measurements of the shrinking rate of a rising stream of hydrate coated CO₂ droplets released at 800m depth off the coast of California.

Brewer et al. (1998; 1999) investigated the formation of a CO₂ hydrate through a series of in situ experiments, and Rehder et al. (2004) have shown that true "storage" as a hydrate is not possible. The essential condition for hydrate stability is the equality of chemical potential in all three phases (water, solid, and hydrate guest molecule). Since normal sea water is very much under-saturated with respect to CO₂, the hydrate exposed to deep waters will soon dissolve. The boundary condition is set by the formation of a diffusive CO₂ saturated boundary layer, and the rate of dissolution is governed by the thickness of this layer (Santschi et al., 1991), and is in proportion to the square root of local water velocities (Hirai et al., 1995). Aya et al. (1991, 1993, 1995) measured this dissolution rate by a high-pressure loop. The balance of the formation and dissolution rates of hydrate determines the thickness of the hydrate skin.

The study of the dissolution of a mass of liquid CO₂ placed on the ocean floor is therefore not an easy problem, although laboratory experiments provide some guidance (Aya et al., 1995B; Fujioka et al., 1995; Masutani et al., 1995; Nishikawa et al., 1995; Shindo et al., 1995; Uchida et al., 1995). The first experimental challenge is to safely contain and precisely deliver the material to the deep ocean. Brewer et al. (1999) reported development of an accumulator system, carried by an ROV, which permits active experimental control to compensate for the large volume changes undergone by the highly compressible liquid CO₂ during descent to the sea floor. This approach has been used in modified form (Peltzer et al, 2003; Brewer et al, 2003) to accommodate larger volumes ever since.

Characteristics of liquid CO₂ and the reaction with sea water.

The physical behavior of CO₂ under oceanic conditions is well known. At shallow depths CO₂ is in the gas phase, and it condenses to the liquid state at depths of ~400m depending upon the local temperature regime. In typical ocean waters CO₂ will form a solid hydrate at depths as shallow as 350m; in a warm water basin such as the Mediterranean or Red Sea, the thermal forces will always exceed the hydrate van der Waals forces, and no hydrate will form. Whether hydrate forms or not, the boundary condition on the sea water side of the interface is set by the solubility of CO₂ at the local pressure and temperature. Liquid CO₂ is highly compressible; sea water is highly incompressible (Fig. 1). The net result is that a density reversal occurs so that CO₂ is buoyant above about 2700m depth, is neutrally buoyant at about 2800m depth, and forms a sinking plume below about 3000m depth, with the approximations due to locally varying oceanic T and P.

Once CO₂ is dissolved in sea water a complex series of processes occurs. The first step is slow hydration (Johnson, 1982; Soli and Byrne, 2002) of the CO₂ molecule to form H₂CO₃, followed by rapid ionic exchanges to form the well-known HCO₃⁻ – CO₃²⁻ equilibria established at the local pH. Yet so slow is the hydration-dehydration step measured at 1 atmosphere that at temperatures of 1 – 2 degrees it may take tens of minutes for equilibrium to be established, so that in a field experiment local advection may remove the reactants far from the observing site before equilibrium is reached. The effect of pressure on the reaction rates is unknown.

The solubility of CO₂ in sea water at low temperatures and at high pressure (Aya et al., 1997), is far greater than for a normal atmospheric gas (Wiebe et al., 1933) and the low partial molal volume of CO₂ (31 cm³/mol) relative to its molecular weight (44) ensures that CO₂ enriched sea water, at equilibrium, has significantly greater density (Haugan and Drange, 1992). Thus the plume emanating from a local CO₂ source has a complex chemical signature, is possibly not at equilibrium, and may be sufficiently increased in density that plume dynamics are affected.

The surface of the liquid source for the plume is itself complex. The boundary between the liquid CO₂ and sea water is characterized by the existence of a hydrate skin with unusual properties (Yamane et al., 2000). The surface readily deforms but is not elastic in the normal sense – for relatively slow stretching rates the rate of hydrate re-building renews the surface skin so that continuity is preserved. For faster stretching the hydrate nucleation kinetics are overcome and a simple liquid CO₂ –sea water interface is presented. Although the density of the solid CO₂ hydrate is greater than that of either sea water or liquid CO₂ at depths above 5 km, a thin film may not be expected to sink to the bottom of the fluid because the mechanical strength of the film is much larger than the small gravitational force due to the density difference between CO₂ hydrate and CO₂-saturated seawater (Aya et al., 2004). Only when active convection is induced, either by external mechanical force, such as the shaking normally used in laboratory studies, or by self-induced flow (Brewer et al., 1999) can large-scale solid hydrate formation occur.

Experimental plan.

If deep-ocean CO₂ sequestration is to be considered, then the phenomena described above are the essential features for study. A gravitationally stable pool of CO₂ on the sea floor can only be created at depths below 3000m, however the density difference between CO₂ and sea water at this depth is still very small, and the entire experimental pool could very easily be destabilized. For this reason we selected 4000m depth for the experiment

reported here. This possibly sets a depth record for this class of work, and the increased Δp permits more robust examination of the effects of physical forcing of the interface to create an experimental plume.

The principal concerns over any proposed sequestration strategy are safety, the containment lifetime, and biological impacts. It is the latter that has drawn most attention (Auerbach et al., 1997; Tamburri et al., 2000; Seibel and Walsh, 2001), and the fate of organisms exposed to a plume of low pH-high CO_2 water must be investigated. Yet even if no direct injection of fossil fuel CO_2 takes place, we are faced with the inevitable prospect of a significantly lower pH ocean (Haugan and Drange, 1996; Brewer, 1997) from the already massive surface invasion of the fossil fuel transient. If we are to evaluate the impacts these high CO_2 levels will cause (Cicerone et al., 2004) then we must consider controlled experiments in which we artificially elevate the CO_2 levels of the local ocean environment in much the same way that ecosystems on land are exposed to higher atmospheric CO_2 levels (DeLucia et al., 1999; Shaw et al., 2002). Lessons learned here may guide us.

In preparatory work (Brewer et al., 2004) we have investigated the turbulent signature of the pH of a very small-scale plume emitted from the surface of a pool of CO_2 trapped (in an inverted experimental box) at 650 depth. This served to develop deployment technique, and to set the time and space scales required for sensing of the CO_2 plume. It also led to the observation of strikingly large fluctuations in pH close to the CO_2 source, far larger than might be expected from turbulence alone, leading us to speculate that parcels of water with rapidly changing degrees of equilibrium might be passing by the sensor. Here we test this hypothesis further.

In this paper we describe the controlled formation of a plume of CO_2 rich water at great depth by forcing sea water flow over the liquid CO_2 surface. We present the results from sensing of this plume by both pH and conductivity sensors. In a companion paper Hove and Haugan (this volume) analyze the fluid dynamics of the liquid CO_2 surface.

2. Materials and Methods

56L CO_2 accumulator. For this experiment the 56L CO_2 accumulator (Peltzer et al, 2004) was thoroughly re-built. A new carbon fiber reinforced fiberglass barrel was fabricated and the aluminum end-caps and piston were replaced with ones made from titanium to alleviate problems with corrosion. The end-caps and piston were redesigned to eliminate voids on the seawater side, while increasing the depth of the recessed cavity on the CO_2 side to allow for an internal cooling loop. The extended length of the CO_2 end-cap also allowed for a second O-ring seal to solve the leakage problems encountered earlier.

Benthic flume. In order to have more operator control over the plume created during the release experiments, a 'benthic flume' was constructed (Fig. 2). It consisted of a trough for CO_2 150 cm long, 40 cm wide and 25 cm deep; a thruster (driven by a computer controlled brushless DC motor) to generate a variable seawater current along the CO_2 trough; and a wave generator paddle. Both the wave paddle and the thruster were controllable in finite increments by the experimentalist in real-time. A clear panel on the front, and an opaque panel on the back, helped to channel the seawater flow

through the flume and aided in viewing of the CO₂ pool under the various stresses. Power and control of the benthic flume was achieved via the ROV by using an underwater mateable connection.

pH probes and calibration. SBE18 pH sensors (Seabird Electronics, Inc., Bellevue, WA 98005) were used. While these sensors have a nominal depth rating of 1200m, we have found that when they are slowly deployed to depth, they can be used as deep as 4000m. The pH electrodes were calibrated using seawater solutions where the pH had been previously adjusted using concentrated HCl or NaOH to ~6 and ~8 as measured by an IQ240 ISFET pH electrode (IQ Scientific Instruments, Inc., San Diego, CA 92127) that was calibrated using commercially available NBS pH standard solutions.

Seawater recirculation chamber. A small volume (~300 mL) chamber (Fig. 12) was equipped with both a pH sensor and a temperature sensor so that samples of CO₂ enriched seawater could be collected and re-circulated. This allowed the in situ rate of the CO₂ hydration reaction to be studied. A Seabird submersible pump was used to fill, flush and re-circulate seawater in the chamber. Pumping rates on the order of 0.9-1.2L/min were achieved at depth.

3. Experimental Deployment and Operation

The experiment carried out is simple in concept but difficult to execute. The work was carried out over a 3 day period from 25 – 27 October, 2003. Day 1 was devoted to deploying the sea floor flume and CTD-pH sensors, partially filling the flume with CO₂, and testing the wave actuator and thruster. Day 2 was devoted to an extended series of wave generation and water flow experiments. Day 3 was devoted to finalizing the fluid and plume tests, and safe recovery of the equipment.

Deployment.

The complex set of equipment, including the flume, and recording CTD-pH frames, was deployed on a large “elevator” equipped with an acoustic beacon, and with floatation adjusted to sink at a speed of a few meters per minute. This was allowed to sink in free fall to the bottom at 3941m depth. This was followed by an ROV dive, and acoustic location of the deployed materiel, which was found buoyed upright on a relatively flat sea floor. The equipment was removed from the elevator by a series of ROV manipulator operations, and set up on the sea floor with the long axis of the flume in line with the observed local current, and the thruster motor upstream. The three recording CTD frames were placed in line downstream of the flume, slightly offset from each other in an effort to avoid shielding of the flow by the measurement structure. The frame placing was: Unit 1 = 0.5m from the end of the CO₂ flume, Unit 2 = 2m distant, and Unit 3 = 5m distant. The local environmental conditions remained stable during the course of the experiment at S‰ = 34.568, and T = 1.492°C.

Filling

The flume was partially filled with 40 L liquid CO₂ on day 1 of the experiment following procedures detailed in Peltzer et al. (2004) to ensure maximum delivered volume. The filling was completed with a second delivery on day 2, whereupon the CO₂ surface was approximately 5 cm below the lowest side of the flume.

Formation of a plume

The liquid CO₂ surface was investigated in three modes during the experiment.

- 1) Quiescent, with only local ocean water motions producing the plume. This replicates to some extent the results from the sea floor CO₂ experiments reported in Barry et al. (2004), and it is the condition recorded during the night hours when the vehicle was not present. The pH signal at a point records the plume only when the local current directs it by the sensor.
- 2) With gravity waves generated at the CO₂ surface by a flapper. This does not cause a directional plume, and these data are not the primary focus of this paper.
- 3) With seawater forced over the surface at varying speeds as controlled by the thruster motor. The thruster/flume system was calibrated in a test tank at one atmosphere and room temperature several days before deployment. These results calibration data are shown in Figure 3.

4. Results

Although three experimental days were available, a technical error in setting the CTD-pH unit recording rates led to premature memory filling and only 2 days of plume sensing with the recording CTD systems were obtained, albeit at high temporal resolution.

Observing the liquid CO₂ surface processes.

The boundary layer processes were observed in four ways: visually with the ROV camera, by careful placement of a pH electrode controlled by the vehicle robotic arm, by pH sensitive dye injection, and by water sampling.

- i) The visual observation of the surface showed the pronounced effect of the wave motions created both by the flapper and thruster systems. The fluid dynamical analysis of the motions induced is discussed in a separate paper by Hove and Haugan (this volume). We were careful not to exceed the critical velocity at which droplets of liquid were torn from the surface and advected past the downstream sensors. These can collect as a pool on the sea floor adjacent to the sensors.

We were routinely able to observe the formation of a hydrate skin on the liquid surface. Most often a thin skin of hydrate formed upon a globule of liquid CO₂, and the resulting increase in density was very small. Moreover full hydrate cage occupancy is difficult to achieve, and vacant cages produce a positive buoyancy effect. We observed a raft of floating hydrate due to these effects forming at the downstream end of the flume in all our experiments. As the current velocity increased the liquid surface showed no visual sign of hydrate presence, suggesting that the nucleation rate was slower than the rate at which fresh liquid CO₂ was supplied to the interface. As soon as the flow was turned off an opaque skin of hydrate propagated along the surface from the downstream end where the mass of hydrate had accumulated.

- ii) The conventional tool for probing the plume is a glass pH electrode. Profiling with a pH electrode above the CO₂ pool was carried out by carefully positioning the sensor with the vehicle robotic arm. This was challenging for vehicle ergonomic reasons; it was not possible to have calibrated movement and positioning, and thus the distance between electrode tip and liquid CO₂ surface was obtained from post-cruise analysis of the video images. The record obtained from probing the boundary layer in the static condition after an overnight, unperturbed, period is shown in Figures 4 A and B. Only background ocean values of pH (7.72) are observed until the electrode is within 1 cm of the CO₂ surface. On touching the liquid CO₂ surface (and presumably trapping a thin aqueous boundary layer at the electrode surface) pH values of 4 were recorded. By pressing the electrode into the pool, thus creating a depression in the surface filled with CO₂ enriched sea water, a pH as low as 3 was recorded. It is very likely that the influence of the non-aqueous liquid CO₂ surface was affecting the electrode readings, and that these cannot be regarded as true pH values. Rather they are indicators of strong gradients present in a very thin boundary layer.
- iii) Injection of a phenol red indicator into the water flowing through the thruster allowed us both to visualize the flow rates and turbulence in the plume, and the pH changes occurring along the length of the flume surface (Fig. 5). It was not possible to recover from the color camera digital record quantitative estimates of the actual pH values. The qualitative signal showed a thin boundary layer over the CO₂ surface, with gradually changing color of the indicator as it flowed along the liquid CO₂ surface. As the dye stream reached the end of the flume and was mixed upwards into normal sea water on meeting the end wall a strong color change was observed (Figure 5).
- iv) Micro-sampling of the aqueous boundary layer was attempted. We built a unit of 3 evacuated stainless steel cylinders (50 ml volume) with a 5-port sampling valve. A hydraulically driven cam controlled by the vehicle rotated the valve. The stainless steel capillary inlet tube, located near the tip of the pH probe (Fig. 6), was placed close to the CO₂ surface and the sampler was activated. Background ocean TCO₂ values were obtained from 2 Niskin bottles attached to the vehicle; the average of the six samples obtained was 2342 $\mu\text{mol/kg}$.

A total of nine boundary layer samples were obtained for shore-based analysis, with the highest value being only 2391 $\mu\text{mol/kg}$. These small CO₂ enrichments observed are explained by extensive entrainment of surrounding water on opening the evacuated cylinders with a pressure differential of ~ 400 bars.

Observing the plume

The primary data set for observing the plume comes from the pH sensors placed ~ 50 cm beyond the downstream end of the flume. Those results are shown in Fig. 7. The low electrical and thermal noise environment of the deep sea can yield extraordinarily stable in situ pH measurements (Brewer et al., 2000). But the results downstream of a CO₂

source (Brewer et al., 2004) and shown here in Figure 7, exhibit rapid changes far larger than can be attributed to turbulence alone. The relationship between applied thruster power and observed current speed (Figure 3) is very well defined, but the series of velocity/pH tests embedded in Figure 7 show no simple correlation, and we seek answers for this complex behavior.

5. Discussion

The challenge of this experiment is to observe and understand the behavior of a plume of CO₂ rich sea water emanating from a lake of CO₂ placed upon the deep ocean floor. Of the several approaches tried here the only widely accepted one at this time is direct pH sensing, yet the observations shown in Figure 7 are unusual, and indicate caution in interpretation.

The problem is that we do not yet have a sensor for the CO₂ molecule itself. We have visual observations of the liquid surface, but not of the dissolved CO₂ state. We have pH sensors for recording changes in hydrogen ion concentration, and we have conductivity sensors for recording changes in conductance. The relationship of each of these to the CO₂ system state is complex. Moreover in Brewer et al. (2004) we drew attention to the problem that local disequilibrium in the near field CO₂ system might cause due to the well-known slow hydration kinetics (Johnson, 1982; Soli and Byrne, 2002). Here we investigate this problem further.

Direct observations of CO₂ system disequilibrium

We have used the flow through pH cell (Figure 12) to trap a volume of sea water in the flow loop to observe the stability of the plume signal. The cell intake tube was held in the vehicle arm and positioned in the flow field so as to draw in water at the desired location in the plume. The valves are operated hydraulically, the total system volume is about 460 ml, and the flow rate of the pump is about 2 L/min. In Figure 13 we show the results of two experiments with this system. In each case there is a rapid drop in pH from the oceanic background value of 7.88, and from the unstable plume signal of about 7.6, to a new stable reading of ~6.8. The drop in pH is extraordinarily rapid, and the new equilibrium value is reached in about 30 seconds.

Sensing of the plume – pH and conductivity

The above observation of significant disequilibrium in the plume CO₂ system is also apparent in the comparison of the pH and conductivity records obtained. The record of plume advection past the pH sensors deployed at the end of the flume is shown in Figures 7 and 8. The three pH sensors on each frame record hydrogen ion concentration, but the single conductivity sensor also records the events as perturbations to the local conductivity as water rich in a complex mixture of CO₂ system species flows by. In Figure 9 we show a fragment of the data (for clarity) in which the conductivity signal is also displayed. It is clear that although the electrode records a drop in pH, and therefore an increase in HCO₃⁻, the equivalent conductivity shows a decrease. The effect of added HCO₃⁻ is to increase conductivity (Brewer and Bradshaw, 1975); that effect is apparently being offset by a larger opposing signal of an undissociated (non-conducting) species. However we also observe some large pH spikes with no equally large change in

conductivity and the signals are therefore confusing. This is consistent with the flow cell experiments, and it must result from the passage of parcels of water with different time histories and thus different degrees of hydration as they flow by the sensors. What is most unusual is the rapidity of these changes.

Comparison of the pH and conductivity records

In contrast to the brief pH flow cell experiment, the signals recorded on the paired pH and conductivity sensors (Figure 9) cover a large part of the observing period. In order to recover information from these complex signals of a rapidly fluctuating field we must make some approximations.

i) The theoretical analysis of the conductivity changes in sea water from the CO₂ system was reported by Brewer and Bradshaw (1975). The basis for calculating the change in conductivity is to use the partial equivalent conductances (Λ_i) of the appropriate chemical species where

$$\Lambda_i = 1000v \delta K / \delta C_i + V_i K \quad (1)$$

where v is the specific volume of the solution reported, K is the electrical conductivity, and V_i and C_i are the partial equivalent volume and concentration of the added electrolyte i .

At equilibrium the primary effect of adding small quantities of CO₂ to normal sea water is to consume carbonate ion and produce bicarbonate as in:

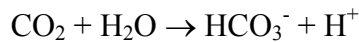


A change in conductance of sea water by 2.5% corresponds to a 1‰ salinity change. For the addition of small quantities of CO₂ to sea water, with full conversion to bicarbonate ion, Brewer and Bradshaw (1975) give

$$\Delta S_{\text{‰}} = 0.030 \text{ per mmol CO}_2/\text{kg} \quad (3)$$

with the increase in bicarbonate ion producing an increase in conductivity.

But the increases in TCO₂ produced here are large, and the small quantities of CO₃⁼ are soon overwhelmed (Figure 9). The reaction is then simply



Substituting the value for $\Lambda_{\text{NaHCO}_3^{-}}$ from Connors and Weyl (1968) we then find that

$$\Delta S_{\text{‰}} = 0.060 \text{ per mmol CO}_2/\text{kg} \quad (4)$$

and we use this value as a useful approximation for our analysis of the data.

If equilibrium is not achieved, and the dominant species is undissociated CO_2 (aq) then the effect is to dilute the salts passing by the sensor; in normal deep sea water dissolved silicate and the atmospheric gases show this effect (Brewer and Bradshaw, 1975). It is not possible to distinguish between the un-dissociated species CO_2 (aq) and H_2CO_3 and these are commonly summed as the concentration of a hypothetical species, CO_2^* (Lueker et al., 2000). The conductance effect is due to the volume fraction (ϕ) of the obstructing electrolyte, and the ratio Λ/Λ° lies between the limits $1-\phi/2$ and $1-5\phi/2$, with the latter being the value for simultaneous validity of Stokes' Law and Einsteins' equation for the viscosity (Stokes and Mills, 1965).

A numerical estimate of ϕ for CO_2^* in sea water is not available, nor is any information on the effect of pressure on this quantity. The effect on conductance of the normal atmospheric gases (N_2 , O_2) is $\sim 1.02 \times 10^{-5} \text{ ohm}^{-1} \text{ cm}^{-1} / \text{mmol/kg}$, or a change of $-0.02\% / \text{mmol/kg}$, and thus if we assume a similar relationship for the un-hydrated CO_2 molecule then a -1% change in conductivity indicates a change of ~ 50 millimolar CO_2^* passing by the sensor.

If the fluid passing by our sensor is close to equilibrium we will see a lowering of pH and an increase in conductivity. If the plume is far from equilibrium we will see a drop in pH from the fraction of CO_2 that has become ionized, but a decrease in conductivity from the dilution effect of the larger quantity of CO_2^* . The signals we observe fall between these extremes, depending upon the travel time to the sensors.

We use these relationships here to examine the data obtained from the pH and conductivity record of the experiment. We cannot expect the sensors to have truly identical records of the plume; the single conductivity sensor is in an actively pumped flow, and the three pH electrodes are simply passively exposed. However the experimental arrangement was such that the tip of the middle electrode was placed very close to the intake tube of the CTD cell.

The change in total CO_2 content of the water flowing past the conductivity and pH sensors may then be approximated by combining the results as in:

$$\Delta \text{TCO}_2 = \Delta \text{HCO}_3^- + \Delta \text{CO}_2^* \quad (5)$$

The term ΔHCO_3^- may be obtained conventionally from the alkalinity and observed pH data as in:

$$\Delta \text{HCO}_3^- = \frac{\Delta \text{pH}_{\text{measured}}}{\left(\frac{\delta \text{pH}}{\delta \text{HCO}_3^-} \right)_{\text{calculated}}} \quad (6)$$

and the conductivity data is a function of the two competing effects:

$$\Delta \text{Cond}_{\text{measured}} = \left(\frac{\delta \text{Cond}}{\delta \text{HCO}_3^-} \right) \times \Delta \text{HCO}_3^- + \left(\frac{\delta \text{Cond}}{\delta \text{CO}_2^*} \right) \times \Delta \text{CO}_2^* \quad (7)$$

The quantities in the parentheses are known relationships from equations 1- 4 above, and $\Delta \text{pH}_{\text{measured}}$ and $\Delta \text{Cond}_{\text{measured}}$ are the data. The relationship $\delta \text{pH} / \delta \text{HCO}_3^-$ is known from the standard CO_2 system equations. There are three unknowns (ΔTCO_2 , ΔCO_2^* , and ΔHCO_3^-), so a solution is possible.

The strategy was to take the observed pH change, and calculate the change in HCO_3^- . We then use the relationship between conductivity and ΔHCO_3^- to estimate the increase in conductance caused by this species. We then take the observed change (decrease) in conductivity and compute the concentration of CO_2^* by summing the two contributions. We then estimated the total CO_2 increase in sea water flowing past the sensor by adding the ΔHCO_3^- and ΔCO_2^* contributions. The records of the individual ΔHCO_3^- and ΔCO_2^* contributions are shown in Figure 11.

The effects and implications of non-equilibrium conditions

The presence of strong local CO_2 disequilibrium effects was predicted and observed, by the contrasting pH and conductivity record. At 2°C and one atmosphere the e-folding time for CO_2 hydration predicted from the one atmosphere data is 303 seconds, and for dehydration it is 0.37 seconds, thus it is the hydration rate that provides the dominant effect. The result is that the observed boundary layer density is by no means as high as predicted from equilibrium models. Although the partial molal volume of CO_2 is reported as only 31 cm^3 per mol, that value is only achieved after complete reaction with sea water and full hydration. The true partial molal volume of the un-hydrated species is, as mentioned earlier, unknown, since observations of the CO_2 system at dis-equilibrium have not been made.

For advection of water across very large-scale lakes of CO_2 on the ocean floor the increased time scale would move the system closer to equilibrium as plume reactions occur, and the strong density increase predicted and modeled (Fer and Haugan, 2003) would likely be observed.

Our observations also suggest a previously unknown pressure effect on the CO_2 system rate constants in sea water, for although disequilibrium was observed the effects were less striking than estimated from the one atmosphere data. We will address this topic in a later study. Such a pressure dependence may be implied simply by the existence of the volume decrease on hydration of the CO_2 molecule, but possible energy barriers are unknown, and while the pressure dependence of the equilibrium state can be calculated from the partial molal volumes, the rate of change of a reaction can only be determined experimentally.

6. Summary and Conclusions

We have carried out a novel experiment to investigate the formation of a plume of high CO_2 water emanating from a pool of liquid CO_2 on the ocean floor. The plume formation was induced by forcing water flow over the surface of the liquid with a controllable thruster. There have been many models and descriptions of this process in the context of deep ocean fossil fuel CO_2 disposal. Our initial findings substantially modify many of the concepts of such a system. Although the system is far inside the hydrate phase space we did not observe large scale hydrate formation, even under strong physical forcing which induced shearing of the liquid CO_2 interface. Although the density of the CO_2 hydrate is greater than that of the liquid, surface tension forces held what were essentially large globules of the liquid encased in a deformable hydrate skin floating on the liquid surface.

The plume was sensed by both pH electrodes, and by a conductivity sensor. The slow hydration rate of the CO_2 molecule resulted in very large amounts of CO_2 being undetected by the pH electrode, and the far larger component of the near field plume

was detected by a drop in conductivity from dilution of sea salt by the unionized CO₂* species.

While the slow hydration rate was clearly a major factor the Δ pH observed was significant, and this hints at a pressure dependence of the hydration rate constants so that the rate is increased at high pressure. This may be expected from the large decrease in volume for the reaction, but it has not previously been observed.

The total quantity of CO₂ was estimated by converting the observed Δ pH into HCO₃⁻, and calculating the increase in conductance contributed by this species. This was then combined with the decrease in conductance from the unionized molecule to yield a reasonable approximation for the plume signal.

The implications for monitoring a large-scale system are substantial. The use of pH sensors alone will not yield a complete signal, and is likely to underestimate the CO₂ signal in the near field. A sensor for the CO₂ molecule itself would be a great advantage, and newly developed in situ laser Raman spectrometers hold great promise for this (Brewer et al., 2004; Pasteris et al., 2004; White et al., 2005).

Acknowledgements

This paper is in acknowledgement of the extraordinary influence of Nick Fofonoff on ocean science. Nick was a distinguished presence at the Woods Hole Oceanographic Institution throughout the 24 years that the first author of this paper worked there. It was Nick's early work on the thermodynamic properties of sea water that drew attention, and it was Nick that sponsored the work of Alvin Bradshaw on the simple, accurate, and elegant measurement of these properties. From Nick's kindly suggestion sprung a multi-year collaboration between Brewer and Bradshaw, with publication of a 1975 paper in this journal of a paper on chemical perturbations to the conductivity-density-salinity relationship that is still cited today. Thank you, Nick.

We thank two anonymous reviewers for their significant help in revising the manuscript.

This work was made possible by the skilled contributions of the pilots of the ROV Tiburon, and the Captain and crew of the RV Western Flyer. Financial support was provided by the David and Lucile Packard Foundation, by an international research grant from the New Energy and Industrial Technology Organization (NEDO), Japan, and by the U.S. DoE/NETL Ocean Carbon Sequestration Program (Grants No. DE-FC26-00NT40929 and DE-FC03-01ER6305).

References

- Auerbach, D.I., J.A. Caulfield, E.E. Adams, and H.J. Herzog. 1997. Impacts of ocean CO₂ disposal on marine life: I. A toxicological assessment integrating constant-concentration laboratory assay data with variable-concentration field exposure. *Environ. Modeling Assessment*, 2, 345-353.
- Aya, I., K. Yamane and N. Yamada. 1991. Feasibility Study on the Dumping of Carbon Dioxide in deep Sea, *1st Int. Offshore and Polar Engineering Conf.*, Edinburgh, UK, 1, 427-432.

Aya, I., K. Yamane and N. Yamada. 1992. Stability of Clathrate-Hydrate of Carbon Dioxide in Highly Pressurized Water, ASME HTD-Vol.215, *Fundamentals of Phase Change: Freezing, Melting, and Sublimation*, 17-22.

Aya, I., K. Yamane and N. Yamada. 1993. Effect of CO₂ Concentration in Water on the Dissolution Rate of its Clathrate, *Int. Symp. on CO₂ Fixation and Efficient Utilization of Energy*, Tokyo Institute of Technology, 351-360.

Aya, I. 1995A. Dissolution Test of a CO₂ Droplet through Clathrate Hydrate Film at High-Pressure, Handa, N. and T. Ohsumi (eds.). *Direct Ocean Disposal of Carbon Dioxide* Terra Pub, Tokyo, 233-238.

Aya, I., K. Yamane and N. Yamada. 1995B. Simulation Experiment of CO₂ Storage in the Basin of Deep Ocean, *Energy Convers., 2nd Int. Conf. on Carbon Dioxide Removal*, J. Kondo, T. Inui and K. Wasa (eds.), *Energy Convers. Mgmt.*, 36, 485-488.

Aya, I., K. Yamane, and H. Nariai .1997. Solubility of CO₂ and density of CO₂ hydrate at 30 MPa. *Energy*, 22, 263-271.

Aya, I., K. Yamane and K. Shiozaki. 1999. Proposal of Self Sinking CO₂ Sending System: COSMOS, *Greenhouse Gas Control Technologies*, P. Riemer, B. Eliasson and A. Wokaun (eds.), Elsevier, 269-274.

Barry, J.P., K.R. Buck, C.F. Lovera, L. Kuhn, P.J. Whaling, E.T. Peltzer, P. Walz, P.G. Brewer. 2004. Effects of direct ocean CO₂ injection on deep-sea meiofauna. *J. Oceanogr.*, 60, 759-766.

Brewer, P.G. and A. Bradshaw. 1975. The effect of the non-ideal composition of sea water on salinity and density. *J. Mar. Res.*, 33, 157 – 175.

Brewer, P. G.1978. Direct observation of the oceanic CO₂ increase. *Geophys. Res. Lett.*, 5, 997-1000.

Brewer, P.G.1997. Ocean chemistry of the fossil fuel CO₂ signal: the haline signature of "Business as Usual." *Geophys. Res. Lett.*, 24, 1367-1369.

Brewer, P.G., F. M. Orr, Jr., G. Friederich, K. A. Kvenvolden, and D.L. Orange. 1998. Gas hydrate formation in the deep sea: *In situ* experiments with controlled release of methane, natural gas and carbon dioxide. *Energy and Fuels*, 12, 183-188.

Brewer, P.G., G. Friederich, E.T. Peltzer, and F.M. Orr, Jr. 1999. Direct experiments on the ocean disposal of fossil fuel CO₂. *Science*, 284, 943-945.

Brewer, P.G., E.T. Peltzer, G. Friederich, I. Aya, and K. Yamane. 2000. Experiments on the ocean sequestration of fossil fuel CO₂: pH measurements and hydrate formation. *Mar. Chem.*, 72, 83-93.

- Brewer, P.G., E. T. Peltzer, G. Friederich and G. Rehder. 2002. Experimental determination of the fate of rising CO₂ droplets in seawater. *Environ. Sci. Technol.*, **36**, 5441-5446.
- Brewer, P.G., E.T. Peltzer, G. Rehder, R. Dunk, Advances in Deep-Ocean CO₂ Sequestration Experiments. 2003. In: "*Greenhouse Gas Control Technologies*" 1667-1670. J. Gale and Y. Kaya, Eds., Pergamon.
- Brewer, P.G., G. Malby, J.D. Pasteris, S.N. White, E.T. Peltzer, B. Wopenka, J. Freeman, M.O. Brown. 2004. Development of a laser Raman spectrometer for deep-ocean science. *Deep-Sea Res. I*, **51**, 739-753.
- Brewer, P.G., E.T. Peltzer, I. Aya, P. Haugan, R. Bellerby, K. Yamane, R. Kojima, P. Walz, Y. Nakajima. 2004. Small scale field study of an ocean CO₂ plume. *J. Oceanogr.*, **60**, 751-758.
- Cicerone, R., J. Orr, P.G. Brewer, P. Haugan, L. Merlivat, T. Ohsumi, S. Pantoja, and H.O. Poertner. 2004. The ocean in a high CO₂ world. *Eos*, **85**, 351-353.
- Cole, K.H., G.R. Stegen and D. Spencer. 1993. The Capacity of the Deep Oceans to Absorb Carbon Dioxide, *IEA Carbon Dioxide Disposal Symposium*, Oxford, UK.
- Connors, D.N. and P.K. Weyl. 1968. The partial equivalent conductances of salts in sea water and the density/conductance relationship. *Limnol. Oceanogr.*, **13**, 39-50.
- DeLucia, E. H., J.G. Hamilton, S.L. Naidu, R.B. Thomas, J.A. Andrews, A. Finzi, M. Lavine, R. Matalama, J.E. Mohan, G.R. Hendrey, and W.H. Schlesinger. 1999. Net primary production of a forest ecosystem with experimental CO₂ enrichment. *Science*, **284**, 1177- 1179.
- Fer, I. and P. M. Haugan. 2003. Dissolution from a liquid CO₂ lake disposed in the deep ocean. *Limnol. Oceanogr.*, **48**(2), 872-883.
- Fujioka, Y., M. Ozaki, K. Takeuchi, Y. Shindo, Y. Yanagisawa and H. Komiyama. 1995. Ocean CO₂ Sequestration at the Depths Larger than 3700 m, *2nd Int. Conf. on Carbon Dioxide Removal*, J. Kondo, T. Inui and K. Wasa (eds.), Energy Convers. Mgmt, **36**, 551-554.
- Handa, N. and T. Ohsumi. 1995. *Direct Ocean Disposal of Carbon Dioxide* Terra Pub, Tokyo, 274 pp.
- Haugan, P.M. and H. Drange. 1992. Sequestration of CO₂ in the deep ocean by shallow injection. *Nature*, **357**, 318-320.
- Haugan, P. and H. Drange. 1996. Effects of CO₂ on the ocean environment. *Energy Convers. Mgmt.*, **37**, 1019-1022.

Hirai, S., K. Okazaki, N. Araki, H. Yazawa, H. Ito and K. Hijikata. 1995. Dissolution and Diffusion Phenomena of Liquid CO₂ in Pressurized Water Flow with Clathrate-Hydrate at the Interface, *Int. Conf. on Technologies for Marine Environment Preservation*, Tokyo, 2, 901-905.

Intergovernmental Panel on Climate Change (IPCC). 1990. Climate Change: The IPCC Scientific Assessment. Cambridge University Press, 364 pp.

Intergovernmental Panel on Climate Change (IPCC). 1995. Climate Change 1995: The Science of Climate Change. Cambridge University Press. 372 pp.

Johnson, K.S. 1982. Carbon dioxide hydration and dehydration kinetics in sea water. *Limnol. Oceanogr.*, 27, 849-855.

Kimuro, H., F. Yamaguchi, K. Ohtsubo, T. Kusayanagi and M. Morishita, 1993, CO₂ Clathrate Formation and its Properties in a Simulated Deep Ocean, *Energy Convers. Mgmt.*, 34, 1089-1094.

Kobayashi, Y. and K. Sato. 1995. Formation of CO₂ Hydrate and Disposal in the Ocean, *Int. Conf. on Technologies for Marine Environment Preservation*, Tokyo, 2, 896-900.

Lueker, T.J., A.G. Dickson, and C.D. Keeling. 2000. Ocean pCO₂ calculated from dissolved inorganic carbon, alkalinity, and equations for K₁ and K₂: validation based on laboratory measurements of CO₂ gas and seawater at equilibrium. *Mar. Chem.*, 70, 105-119.

Marchetti, C. 1977. On geoengineering and the CO₂ problem. *Climatic Change*, 1, 59-68.

Pasteris, J.D., B. Wopenka, J.J. Freeman, P.G. Brewer, S.N. White, E.T. Peltzer, G. Malby. 2004. Spectroscopic successes and challenges: Raman spectroscopy at 3.6km depth in the ocean. *Appl. Spectrosc.*, 58 (7), 195A – 208A.

President's Council of Advisors on Science and Technology (PCAST). Report to the President on Federal Energy Research and Development for the Challenges of the Twenty-First Century.

Masutani, S.M., C.M. Kinoshita, G.C. Nihous, T. Ho and L.A. Vega. 1993. An Experiment to Simulate Ocean Disposal of Carbon Dioxide, *IEA Carbon Dioxide Disposal Symposium*, Oxford, UK.

Masutani, S.M., C.M. Kinoshita, G.C. Nihous, T. Teng, L.A. Vega and S.K. Sharma. 1995. Laboratory Experiments of CO₂ Injection into the Ocean, Handa, N. and T. Ohsumi (eds.). In "*Direct Ocean Disposal of Carbon Dioxide*" Terra Pub, Tokyo, 239-252.

Morishita, M., K.H. Cole, G.R. Stegen and H. Shibuya. 1993. Dissolution and Dispersion of a Carbon Dioxide Jet in the Deep Ocean, *IEA Carbon Dioxide Disposal Symposium*, Oxford, UK.

Nakashiki, N., T. Ohsumi and K. Shitashima. 1991. Sequestering of CO₂ in a Deep-Ocean -- Fall Velocity and Dissolution Rate of Solid CO₂ in the Ocean, *CRIEPI Report, EU91003*, pp.1-19.

Nishikawa, N., M. Ishibashi, H. Ohta, N. Akutsu and M. Tajika. 1995. Stability of Liquid CO₂ Spheres Covered with Clathrate Film When Exposed to Environment Simulating the Deep Sea, *2nd Int. Conf. on Carbon Dioxide Removal*, J. Kondo, T. Inui and K. Wasa (eds.), *Energy Convers. Mgmt.*, 36, 489-492.

Ohgaki, K., Y. Makihara and K. Takano. 1993. Formation of CO₂ Hydrate in Pure and Sea Waters, *J. of Chemical Engineering of Japan*, 26, 558-564.

Ozaki, M., N. Murakami, Y. Fujioka, T. Tanii and Y. Kawada. 1993. Preliminary Investigation on Carbon Dioxide Behavior after Sending into Deep ocean, Mitsubishi Heavy Industries, Ltd., Technical Review, 30,1-7.

Peltzer, E.T., P.G. Brewer, N. Nakayama, P. Walz, I. Aya, R. Kojima, K. Yamane, Y. Nakajima, P. Haugan, J. Hove, and T. Johannessen. 2004. Initial results from a 4km CO₂ release experiment. Prepr. Pap.-Am. Chem. Soc. Div. Fuel Chem., 49 (1), 429-430.

Rehder, G., S.H. Kirby, W.B. Durham, L.A. Stern, E.T. Peltzer, J. Pinkston, and P.G. Brewer. 2004. Dissolution rates of pure methane hydrate and carbon dioxide hydrate in under-saturated seawater at 1000m depth. *Geochim. Cosmochim. Acta.*, 68 (2), 285-292.

Sabine, C.L., R.A. Feely, R.M. key, J.L. Bullister, F.J. Millero, K. Lee, T.-H. Peng, B. Tilbrook, T. Ono, and C.S. Wong. 2002. Distribution of anthropogenic CO₂ in the Pacific Ocean. *Global Biogeochemical Cycles*, doi:10.1029/2001GB001639.

Saito, T., T. Kajishima and R. Nagaosa. 1995. A Gas Lift Advanced Dissolution System for CO₂ Sequestering into the Ocean by Shallow Injection, *Int. Conf. on Technologies for Marine Environment Preservation*, Tokyo, 2, 875-881.

Santschi, P.H., R.F. Anderson, M.Q. Fleischer, and W. Bowler. 1991. Measurements of diffusive sublayer thicknesses in the ocean by alabaster dissolution, and their implications for the measurements of benthic fluxes. *J. Geophys. Res.*, 96, 10641-10657.

Seibel, B.A. and P.J. Walsh. 2001. Potential impacts of CO₂ injection on deep-sea biota. *Science*, 294, 319-320.

Shaw, H. R., E.S. Zavaleta, N.R. Chiariello, E. L. Cleland, H.A. Mooney, and C.B. Field. 2002. Grassland responses to global environmental changes suppressed by elevated CO₂. *Science*, 298 1987-1990.

Shindo, Y., P.C. Lund and H. Komiyama. 1993. Kinetics on Formation of CO₂ Hydrate, *IEA Carbon Dioxide Disposal Symposium*, Oxford, UK.

Shindo, Y., Y. Fujioka, Y. Yanagisawa, T. Hakuta and H. Komiyama. 1995. Formation and Stability of CO₂ Hydrate, Handa, N. and T. Ohsumi (eds.). In "*Direct Ocean Disposal of Carbon Dioxide*" Terra Pub, Tokyo, 217-231.

Soli, A.L. and R.H. Byrne. 2002. CO₂ system hydration and dehydration kinetics and the equilibrium CO₂/H₂CO₃ in aqueous NaCl solution. *Mar. Chem.*, 78, 65-73.

Stegen, G.R., K.H. Cole and R. Bacastow. 1993. The Influence of Discharge Depth and Location on the Sequestration of Carbon Dioxide, *IEA Carbon Dioxide Disposal Symposium*, Oxford, UK.

Stokes, R.H. and R. Mills. 1965. *Viscosity of electrolytes and related properties*. Pergamon Press, 151 pp.

Tabe, T., S. Hirai and K. Okazaki. 1998. Measurement of Clathrate-Hydrate Film Thickness at the Interface between Liquid CO₂ and Water, In "*Greenhouse Gas Control Technologies*", P. Riemer, B. Eliasson and A. Wokaun (eds.), Elsevier, 311-315.

Tsouris, C., Brewer, P.G., Peltzer, E., Walz, P., Riestenberg, D., Liang, L., West, O.R. 2004. Hydrate composite particles for ocean carbon sequestration: field verification. *Environ. Sci. Technol.*, 38, 2470-2475.

Tamburri, M., E.T. Peltzer, G. Friederich, I. Aya, K. Yamane, and P.G. Brewer. 2000. A field study of the effects of CO₂ disposal on mobile deep-sea animals. *Mar. Chem.*, 72, 95-101.

Uchida, T. and J. Kawabata. 1995. Observations of Water Droplets in Liquid Carbon Dioxide, *Int. Conf. on Technologies for Marine Environment Preservation*, Tokyo, 2, 906-910.

White, S.N., P.G. Brewer, E.T. Peltzer. 2004. Determination of gas bubble fractionation rates in the deep ocean by laser Raman spectroscopy. *Mar. Chem.* In Press.

Wiebe, R., Gady, V.L. and Heins, C., 1933. The solubility of nitrogen in water at 50, 75, and 100 deg from 25 to 1000 atmospheres. *J. Am. Chem. Soc.*, 55, 947-953.

Yamane, K., I. Aya, S. Namie and H. Nariai. 2000. Strength of CO₂ hydrate membrane in sea water at 40 MPa. In: "*Gas Hydrates: Challenges for the Future*" *Annals New York Acad. Sci.*, 912, G. Holder and P.R. Bishnoi, Eds., 254-260.

List of Figure Captions

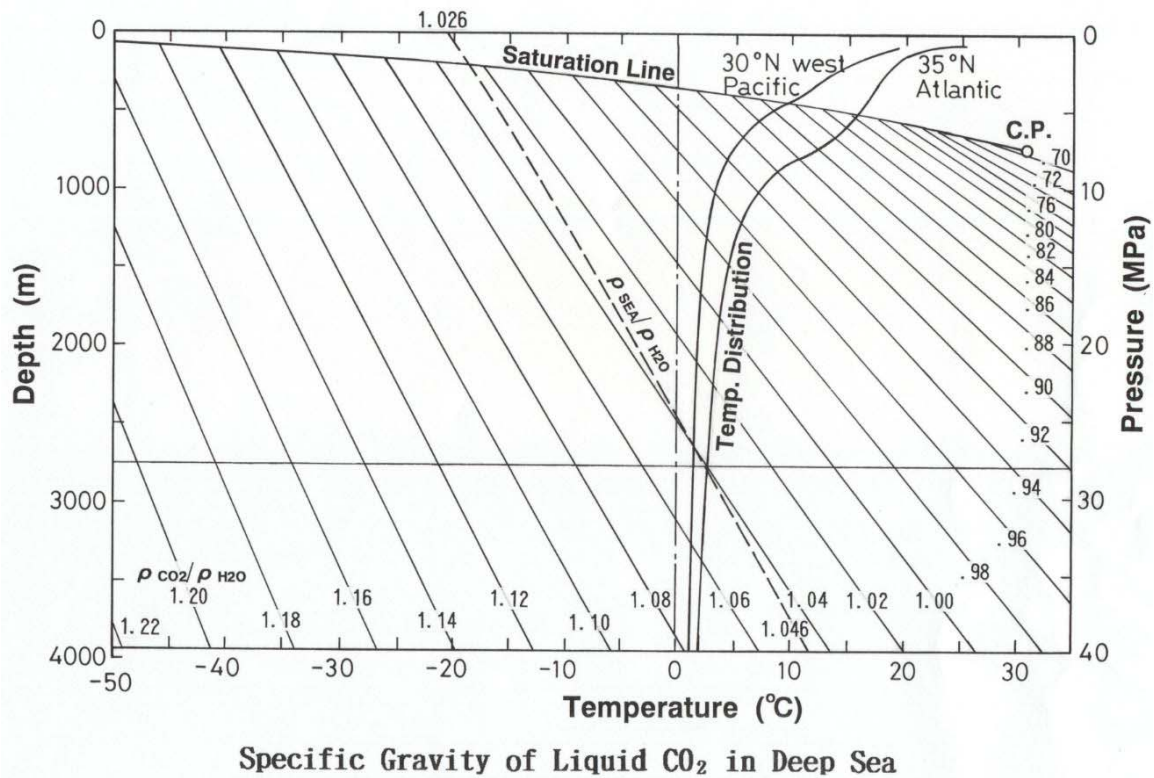


Fig. 1. General illustration of the specific gravity of liquid CO₂ compared to ocean water properties. The high compressibility of the liquid, and the narrow distribution of temperature in the deep sea, results in gravitational stability of a CO₂ pool at depths >3000m.

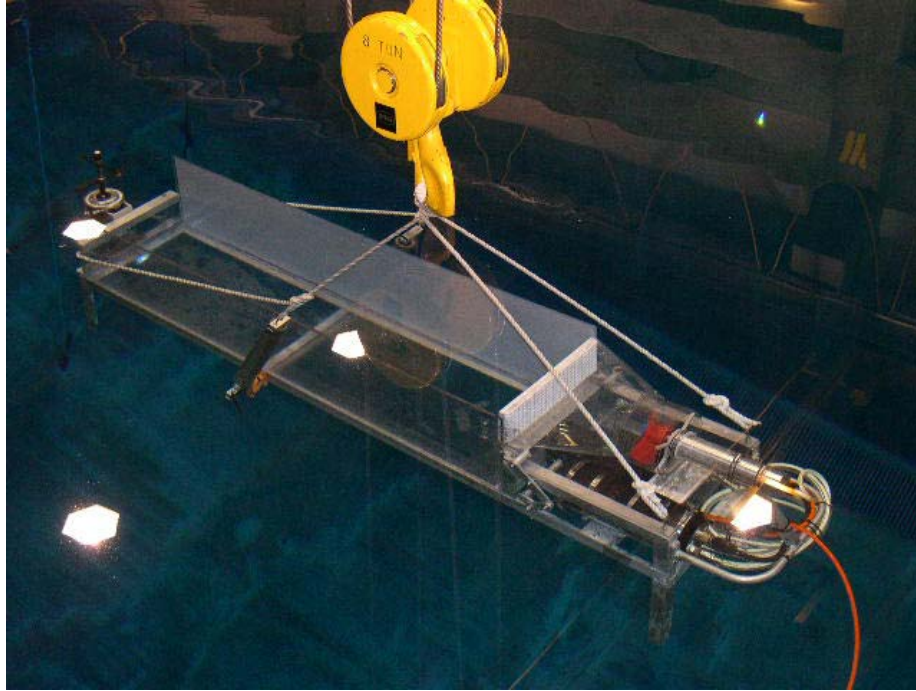


Fig. 2. The experimental flume being lowered into a test tank for velocity calibration of the thruster prior to the experiment. The thruster motor and impeller are at right. A honeycomb screen in front of the thruster helps provide a more laminar flow field. The velocimeter used for calibration is at the far left.

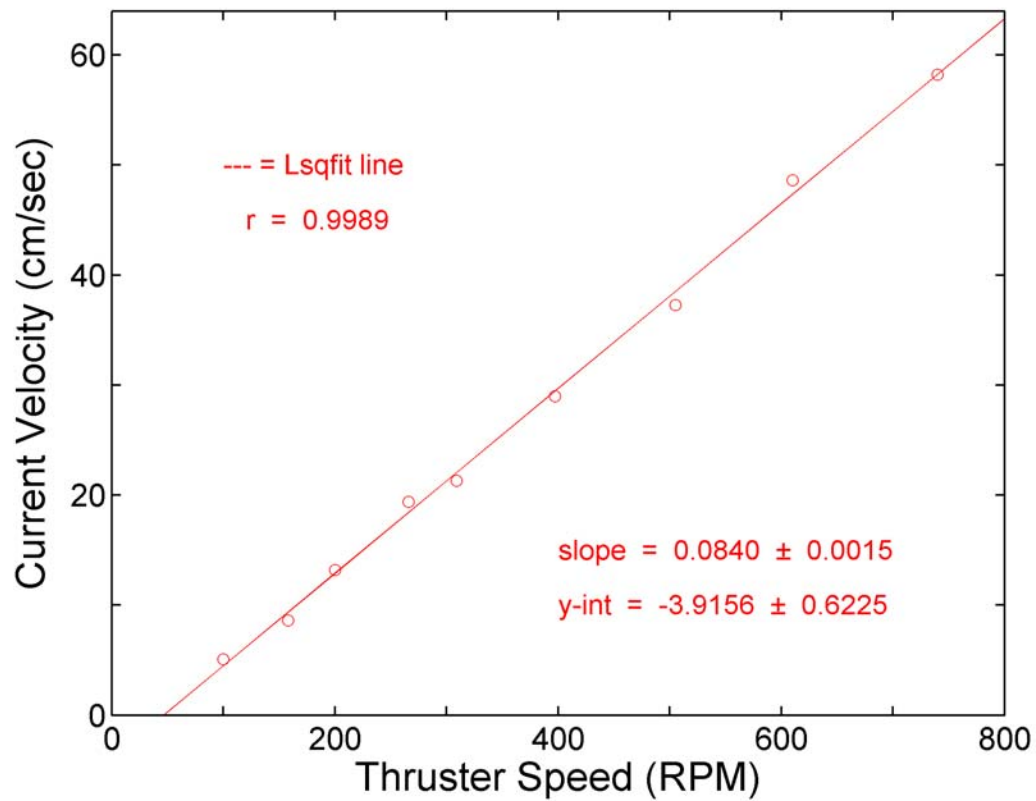


Figure 3. Test tank calibration data for the thruster/flume system used for the experiments. The average velocities for several minute integrals were measured with an rapid response acoustic current meter for applied thruster speed (rpm).

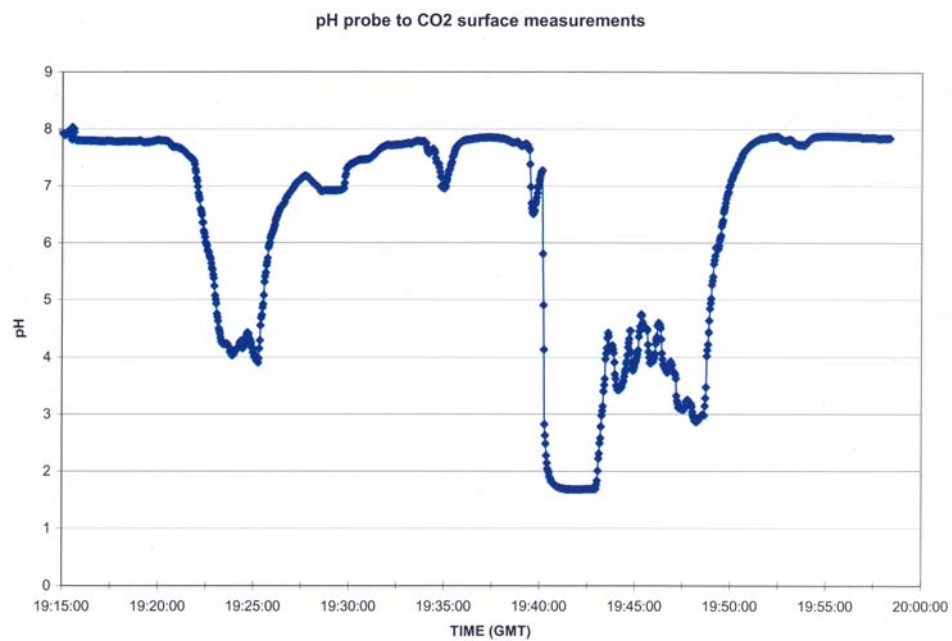


Fig. 4A. Record of experimental probing of the static CO₂ boundary layer in the flume. The electrode is moved up and down in series of motions covering background sea water ~8 cm above the liquid surface (pH= 7.8) to actual probe contact (pH <3.0). pH values of less than 3 are artifacts of contact with the non-aqueous surface and are not valid.

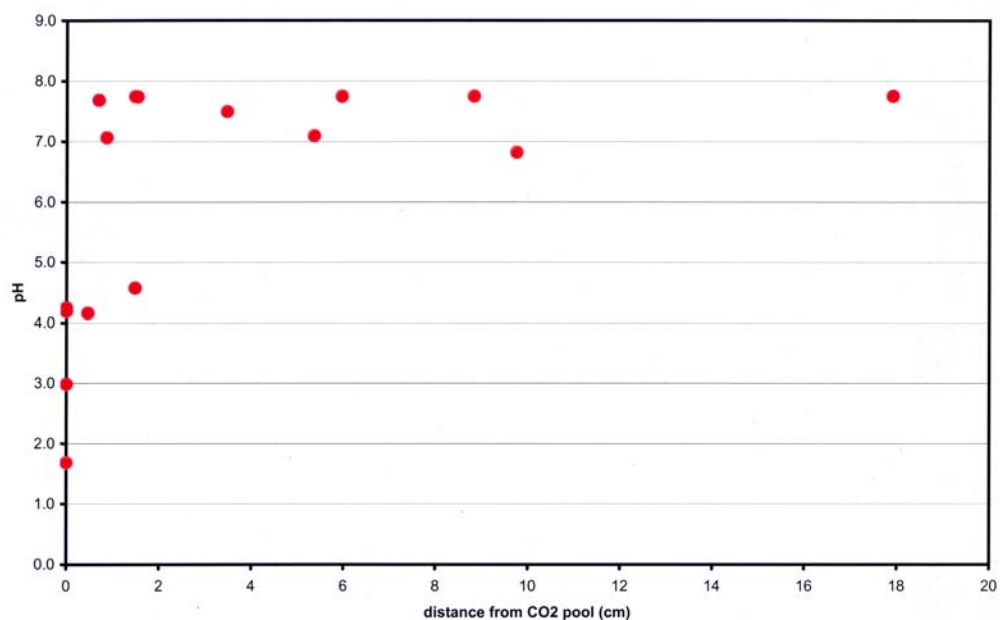


Fig. 4B. Data selected from Fig 3A showing the accumulated record of pH versus distance to the liquid CO₂ surface. The low pH boundary layer, even under very low flow conditions is <1 cm thick; the sensor only responds to the change in hydrogen ion concentration, and does not detect the free CO₂ molecule.

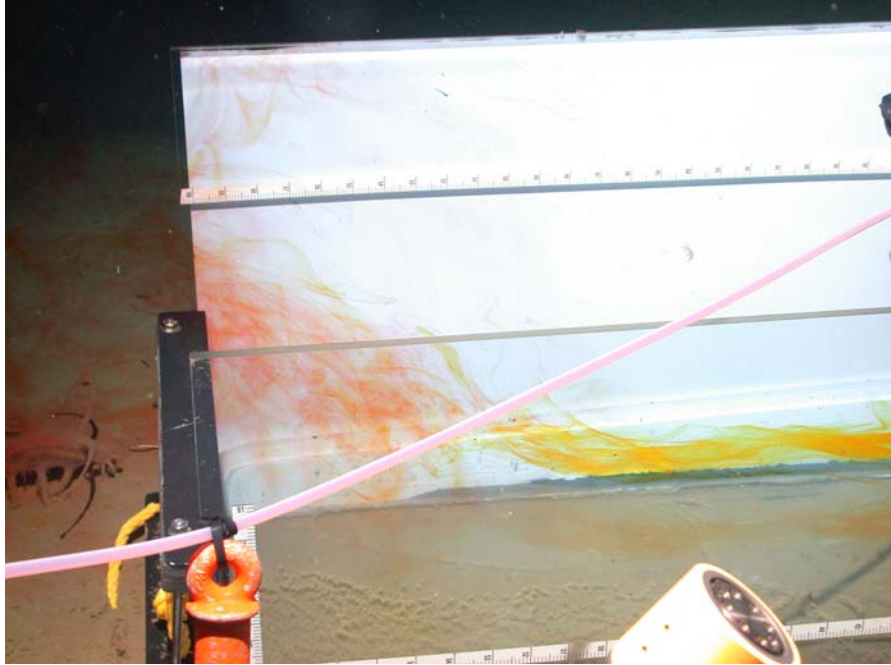


Fig. 5. pH sensitive dye injection into the flume with water velocity $\cong 10$ cm/sec. The yellow dye indicating the low pH boundary layer is being mixed into normal sea water as it exits the end of the flume, and changing to red due to mixing with background ocean water. The dye changes color over the range 8.0 (red) to 6.6 (yellow).

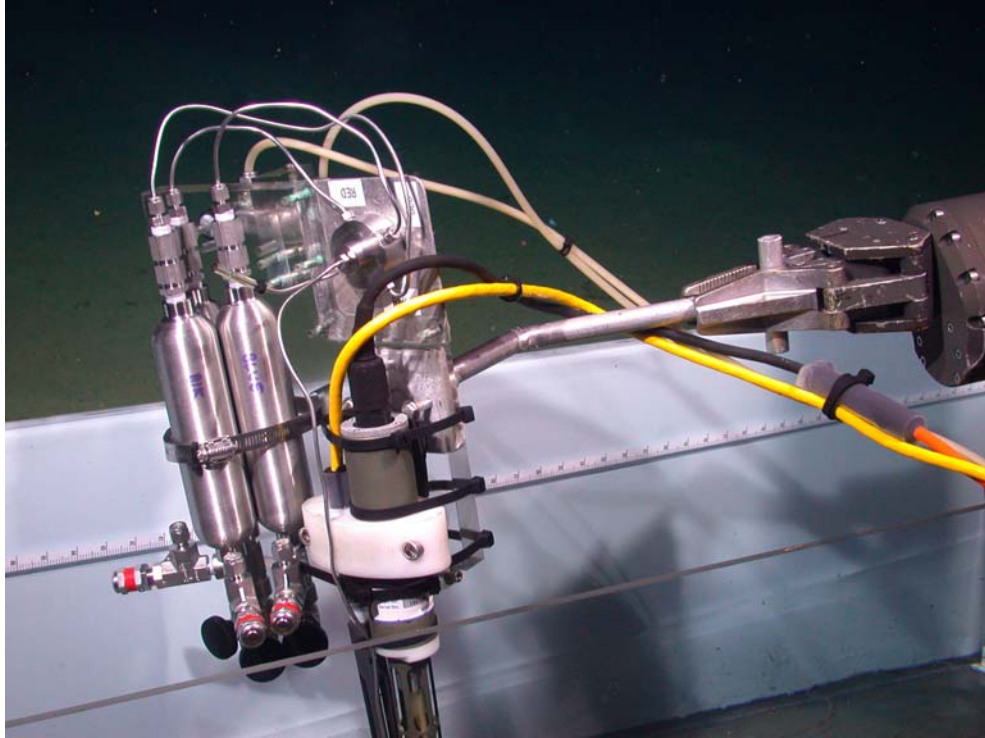


Fig. 6. The evacuated stainless steel cylinder water sampling apparatus, held in the vehicle arm. The fluid intake tube is positioned at the tip of the pH electrode, close to the CO_2 surface.

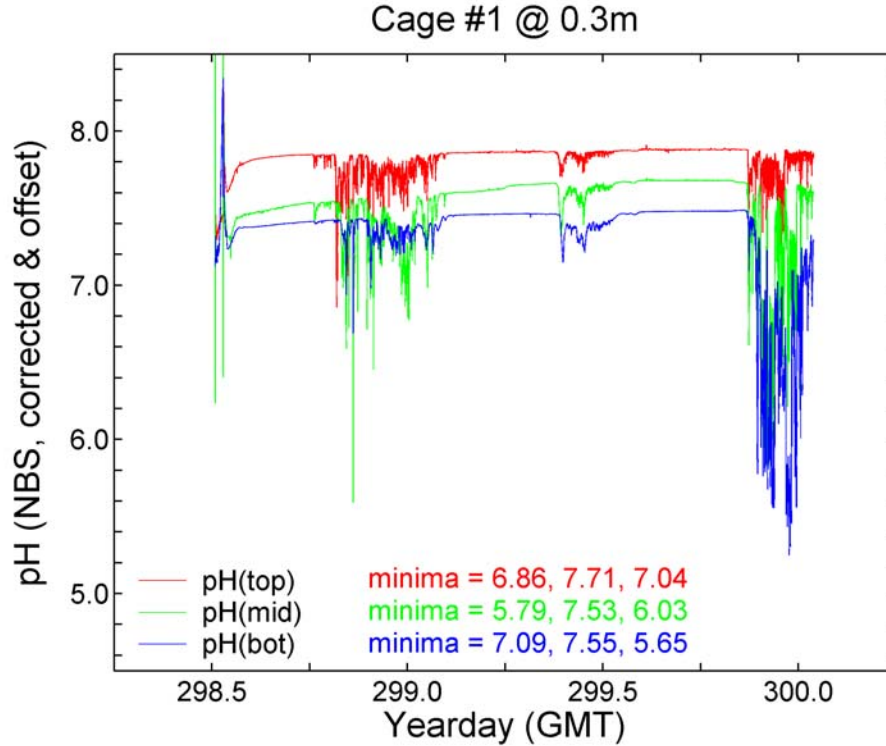


Fig 7. The complete pH record from Frame 1, placed within 50 cm of the end of the flume, with 3 electrodes (data offset for clarity) for the entire experimental period. The smaller perturbations in the center are from natural forcing of flow in the overnight period when the vehicle was not present. The largest signals result from forcing high velocities over the liquid CO₂ surface. The record at the far left is that during passive descent from the surface. The overshoot in pH is an artifact produced by the large and rapid changes in P and T during descent. The electrodes then stabilize at the sea floor conditions. The first series of pH spikes correspond to forced flows of 110 rpm, 1502 rpm, and 95 rpm producing a turbulent flow of low pH water as in Brewer et al. (2004).

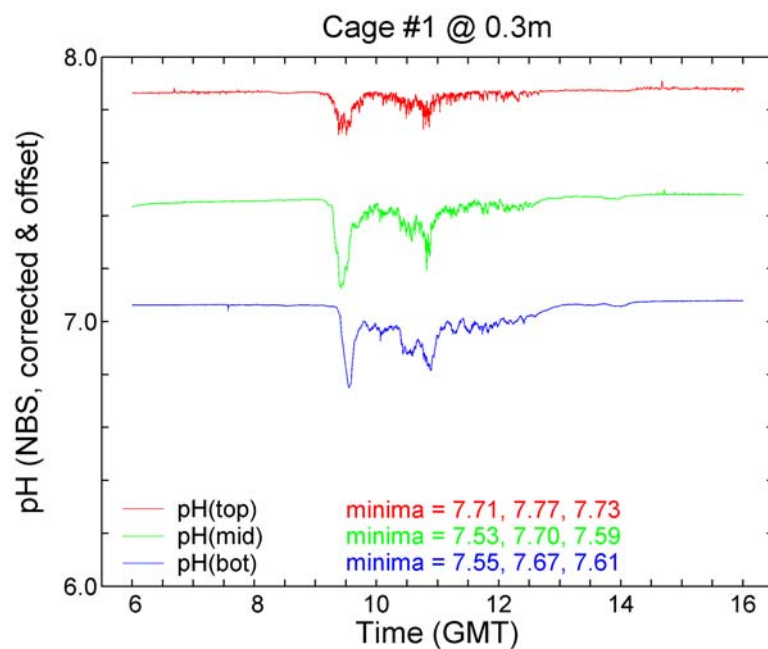


Fig 8. The pH record from Cage 1 closest to the liquid CO₂ source during the unforced low flow (nighttime) period, data offset for clarity. Here there is modest evidence for greater density in the plume with the lowest placed sensor recording a bigger pH signal than the upper one. The middle sensor, placed at the height of the CO₂ surface, records the greatest signal.

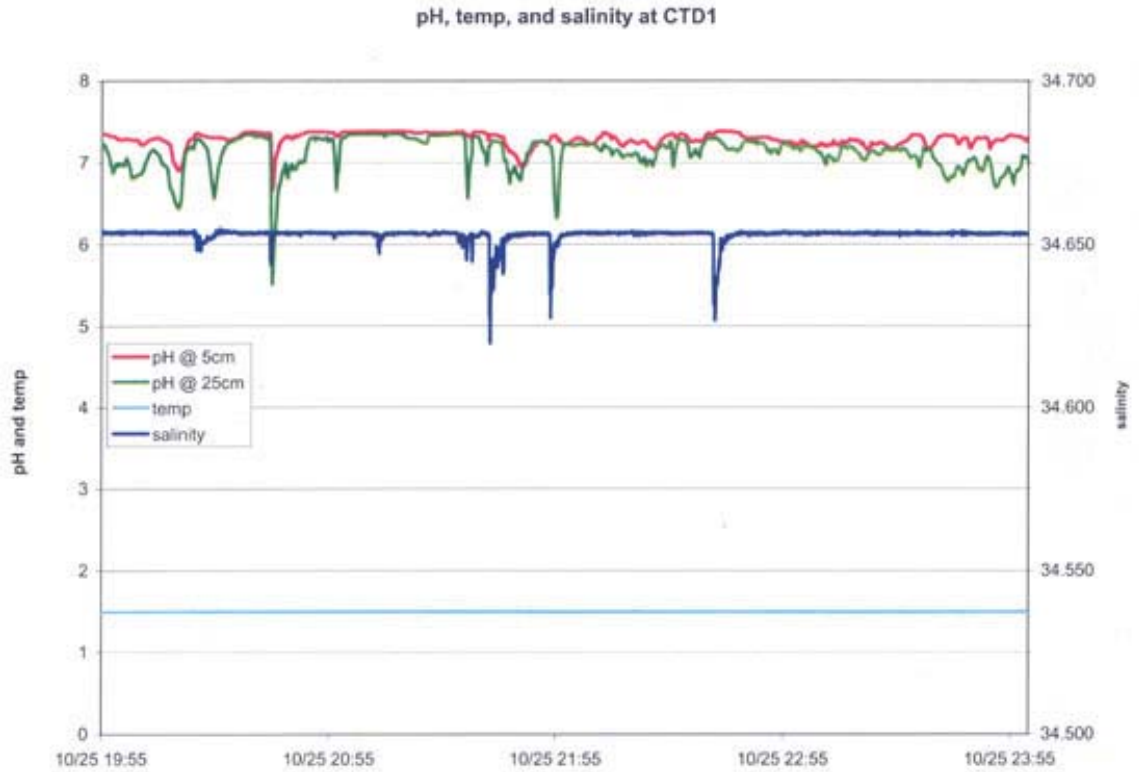


Fig. 9. A brief fragment of the pH and conductivity (expressed as salinity) record obtained from CTD 1 placed closest to the CO₂ source. In each case a low pH spike is accompanied by a decrease in conductivity. This indicates a mixture of CO₂aq and HCO₃⁻ species in the plume, with the CO₂aq being the dominant signal. This results from slow hydration kinetics of the CO₂ molecule in sea water.

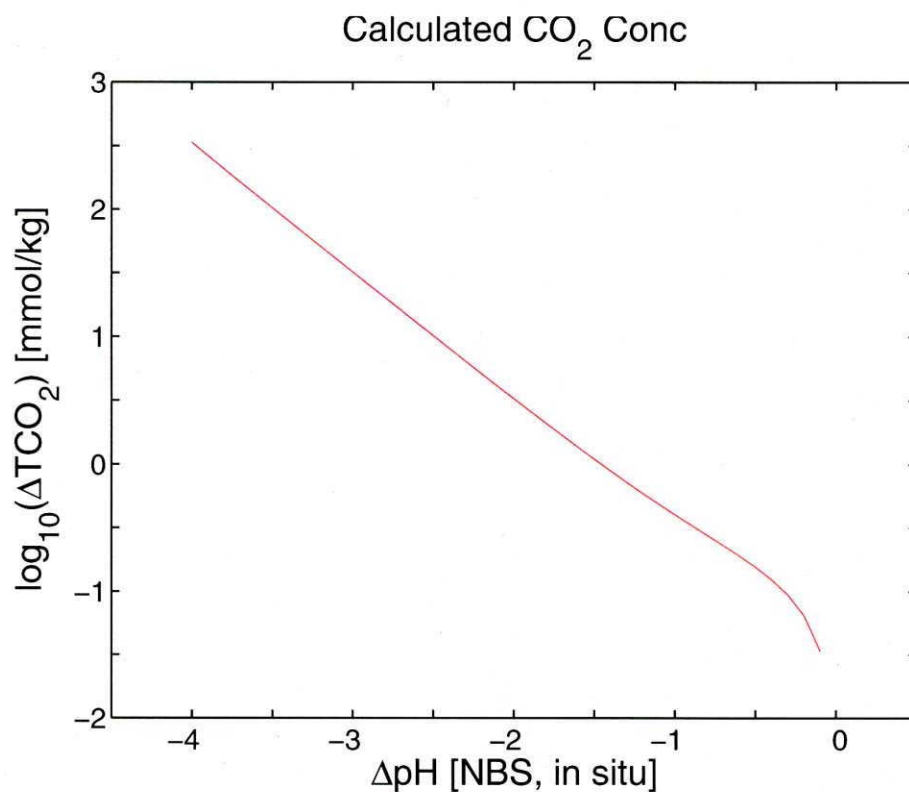


Fig. 10. Relationship between the change in pH and the change in TCO₂ for sea water at the temperature, pressure, and alkalinity of the experimental site. The change in slope near zero ΔpH is from consumption of the $\text{CO}_3^{=}$ ion; once that is removed the slope observed is simply due to HCO_3^- formation.

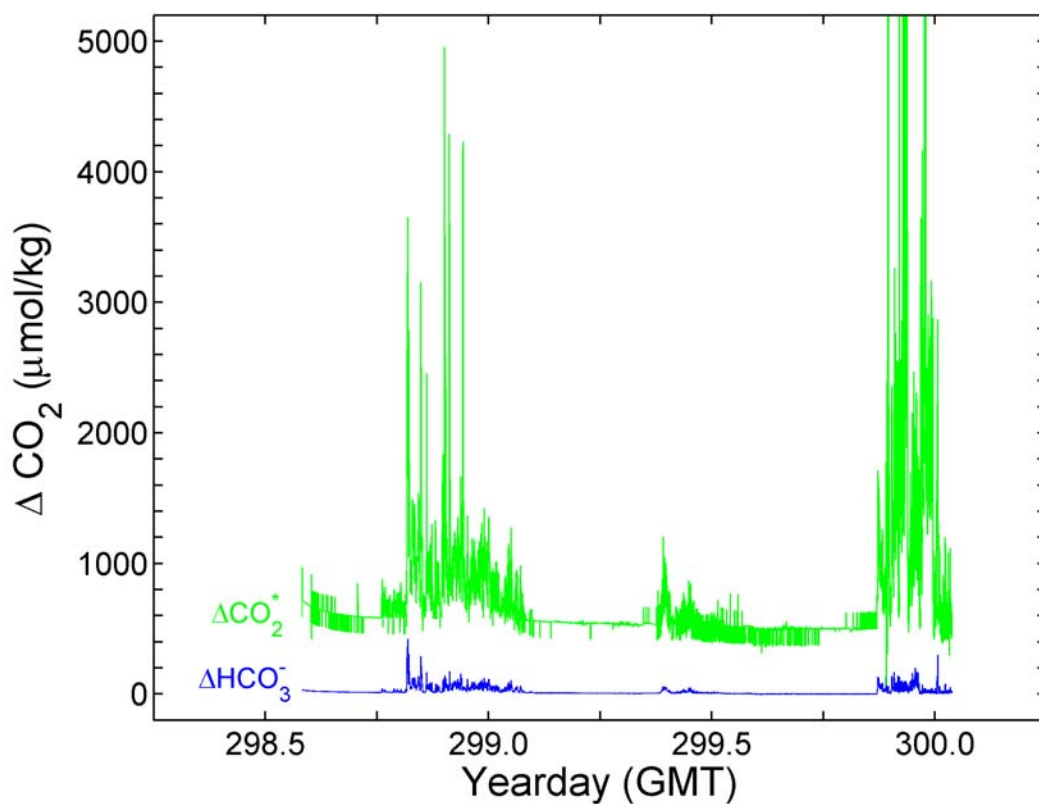


Fig. 11. The record of ΔCO_2^* deduced from the conductivity record, and the change in HCO_3^- as recorded by the middle pH sensor. The ΔCO_2^* signal has been offset by 500 $\mu\text{mol/kg}$ for clarity. Both sensors are about 30cm distant from the CO_2 source. The ΔCO_2^* signal clearly dominates, and the ratio will shift downstream as the hydration-ionization process occurs.

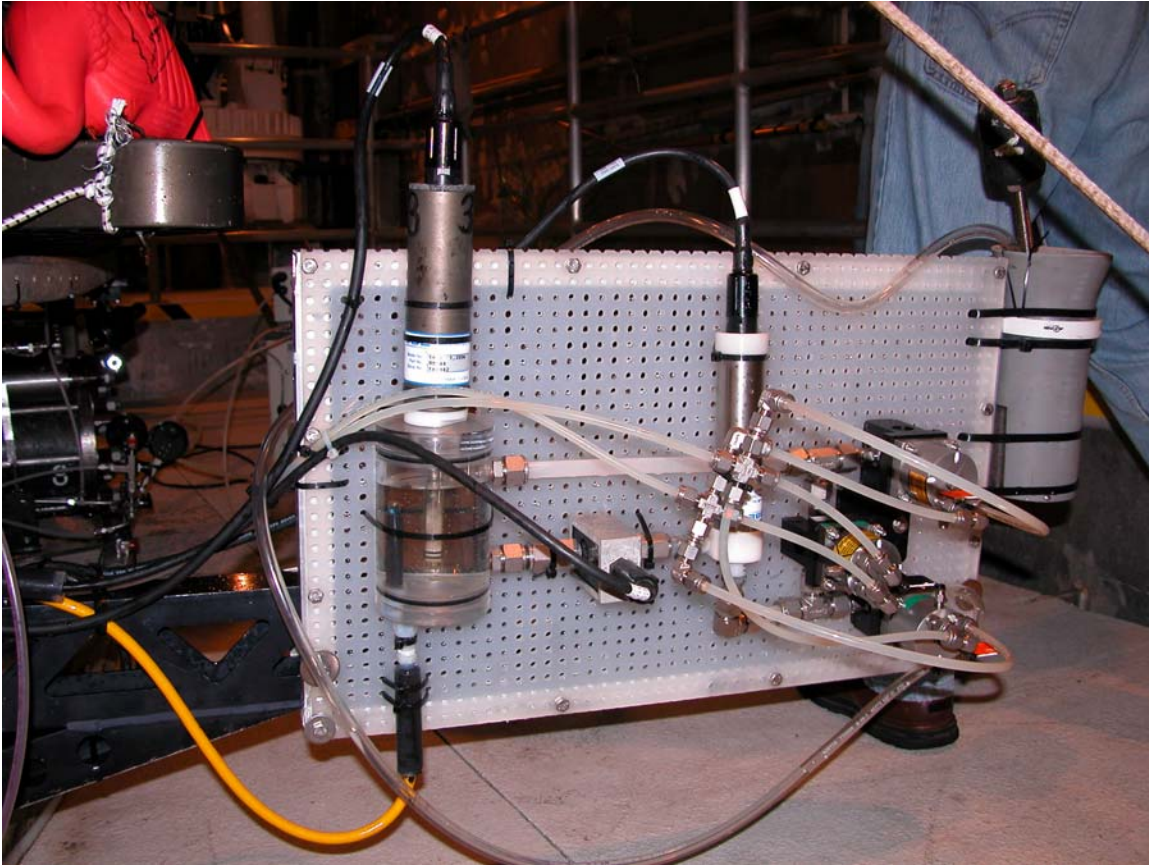


Fig. 12. The looped flow cell used for observing disequilibrium in the CO₂ rich plume. The pH electrode is at left, with the sensor positioned within the flow cell. At center is the pump to provide flow, and two hydraulically controlled valves are at right. These are opened to draw in local sea water which passes by the electrode; closing the valves contains the sample in the flow loop, and allows observation of the time taken to reach equilibrium. The intake tube is stowed in a quiver seen at the far upper right. It is held in the vehicle arm and positioned at the desired location in the flow field.

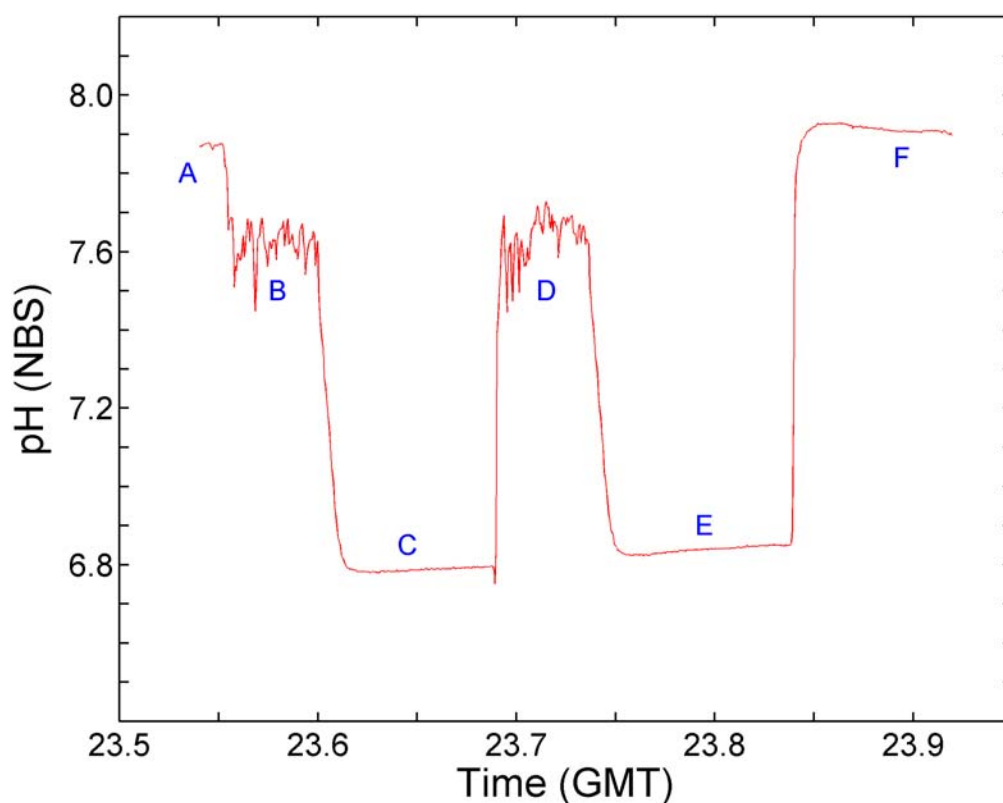


Fig 13. The record of pH from two looped flow experiments carried out on water samples from the CO₂ rich plume. At point A above the flow regime the normal quiescent ocean background signal of 7.88 is observed. The intake tube is then lowered into the flow regime, and large rapidly varying pH signals are observed at point B. Upon closure of the valves the pH signal quickly drops to a pH of 6.8 in region C, and very stable readings are recorded. The sequence is repeated by opening the flow loop, recording once again higher, and rapidly varying, pH signals (D). Upon valve closure the pH again drops (E), and upon raising the intake tube into background sea water and opening the valves normal and stable ocean values are recorded (F). The scale marks on the x-axis are 3 minutes, and the drop to an equilibrium value in the cell takes about 30 seconds.